**Astronomy
&
Astrophysics**

High resolution optical spectroscopy of the N₂-rich comet C/2016 R2 (PanSTARRS)

C. Opitom[1], D. Hutsemékers[2], E. Jehin[2], P. Rousselot[3], F. J. Pozuelos[2], J. Manfroid[2], Y. Moulane[2,4],
M. Gillon[2], and Z. Benkhaldoun[4]

[1] ESO (European Southern Observatory), Alonso de Cordova 3107, Vitacura, Santiago, Chile
e-mail: `copitom@eso.org`
[2] STAR Institute, University of Liège, Allée du 6 Août 19c, 4000 Liège, Belgium
[3] Institut UTINAM-UMR CNRS 6213, Observatoire des Sciences de l'Univers THETA, University of Franche-Comté, BP 1615,
25010 Besançon Cedex, France
[4] Oukaimeden Observatory, High Energy Physics and Astrophysics Laboratory, Cadi Ayyad University, Marrakech, Morocco

ABSTRACT

Context. Early observations of comet C/2016 R2 (PanSTARRS) have shown that the composition of this comet is very peculiar. Radio observations have revealed a CO-rich and HCN-poor comet and an optical coma dominated by strong emission bands of CO^+ and, more surprisingly, N_2^+.

Aims. The strong detection of N_2^+ in the coma of C/2016 R2 provided an ideal opportunity to measure the $^{14}N/^{15}N$ isotopic ratio directly from N_2^+ for the first time, and to estimate the N_2/CO ratio, which is an important diagnostic to constrain formation models of planetesimals, in addition to the more general study of coma composition.

Methods. We obtained high resolution spectra of the comet in February 2018 when it was at 2.8 au from the Sun. We used the UVES spectrograph of the European Southern Observatory Very Large Telescope, complemented with narrowband images obtained with the TRAPPIST telescopes.

Results. We detect strong emissions from the N_2^+ and CO^+ ions, but also CO_2^+, emission lines from the CH radical, and much fainter emissions of the CN, C_2, and C_3 radicals that were not detected in previous observations of this comet. We do not detect OH or H_2O^+, and we derive an upper limit of the H_2O^+/CO^+ ratio of 0.4, implying that the comet has a low water abundance. We measure a N_2^+/CO^+ ratio of 0.06 ± 0.01. The non-detection of NH_2 indicates that most of the nitrogen content of the comet is in N_2. Together with the high N_2^+/CO^+ ratio, this could indicate a low formation temperature of the comet or that the comet is a fragment of a large differentiated Kuiper Belt object. The CO_2^+/CO^+ ratio is 1.1 ± 0.3. We do not detect $^{14}N^{15}N^+$ lines and can only put a lower limit on the $^{14}N/^{15}N$ ratio (measured from N_2^+) of about 100, which is compatible with measurements of the same isotopic ratio for NH_2 and CN in other comets. Finally, in addition to the [OI] and [CI] forbidden lines, we detect for the first time the forbidden nitrogen lines [NI] doublet at 519.79 and 520.03 nm in the coma of a comet.

Key words. techniques: spectroscopic – comets: individual: C/2016 R2 (PanSTARRS)

1. Introduction

Comets are among the most pristine bodies of the solar system. They have undergone little alteration since their formation and their nucleus preserves invaluable clues about the evolution of volatile material within the early solar system at the time of planet formation. Cometary material reveals a diversity of formation processes dating from the early solar system. In particular, isotopic abundance ratios measured in cometary material are very sensitive to local physico-chemical conditions through fractionation processes.

On September 7, 2016 the PanSTARRS (Panoramic Survey Telescope And Rapid Response System) telescope discovered the long period comet C/2016 R2 (PanSTARRS), hereafter R2 (Weryk & Wainscoat 2016). With a period of about 20 000 years and a semimajor axis of 735 au, R2 is a returning object coming from the Oort cloud, meaning that this was not its first passage close to the Sun (Levison 1996). The comet developed a coma at large heliocentric distances ($r \sim 6$ au), and as it was getting closer to the Sun, in December 2017 (at about 3.0 au), it started

to display a very unusual coma morphology in optical images with a lot of structures changing rapidly. This was attributed to ions dominating the emission of the coma and emitting mainly at blue optical wavelengths. Because of its peculiarity, R2 has been the target of numerous telescopes around the world, and at various wavelengths. Radio observations taken near the end of December 2017 revealed a very CO-rich comet with a low abundance of HCN (Wierzchos & Womack 2017). Optical spectra obtained the same month with the 2.7 m telescope of the McDonald Observatory showed that its spectrum was largely dominated by the emission bands of CO^+ and more surprisingly of N_2^+ (Cochran & McKay 2018), confirming that R2 is a very unusual and interesting object.

The detection of N_2 in comets has been a matter of debate for decades. The N_2 molecule itself cannot be detected in cometary spectra in the optical range, but N_2^+ can be observed in this range thanks to the bands of the first negative group ($B^2\Sigma_u^+ – X^2\Sigma_g^+$), the (0,0) bandhead being at 391.4 nm. Before the apparition of R2 only very few detections of N_2^+ emission lines had been reported from ground-based facilities. These

concern very few comets, mainly: C/1908 R1 (Morehouse) (de La Baume Pluvinel & Baldet 1911), C/1961 R1 (Humason) (Greenstein 1962), 1P/Halley (Wyckoff & Theobald 1989; Lutz et al. 1993), C/1987 P1 (Bradfield) (Lutz et al. 1993), 29P/Schwassmann-Wachmann 1 (Korsun et al. 2008; Ivanova et al. 2018), and C/2002 VQ94 (LINEAR) (Korsun et al. 2008, 2014). From these detections only the last two are based on spectra with both good signal-to-noise ratio and good spectral resolution. It also should be pointed out that some spectra might have been contaminated by telluric N_2^+ emission lines. The first in situ detection of N_2 in a comet was done in 67P's coma by the ROSINA mass spectrometer onboard the Rosetta spacecraft (Rubin et al. 2015) (with a N_2/CO ratio of $5.7 \pm 0.66 \times 10^{-3}$).

The N_2/CO ratio provides clues about the formation temperature of comets. Following the first failed attempts to detect N_2^+, several models were developed to explain the N_2 deficit in the coma of comets. Owen & Bar-Nun (1995) considering amorphous ice trapping CO and N_2 gases at temperatures of about 50 K, showed that the N_2/CO abundance ratio in cometary ice would be on the order of 0.06. Iro et al. (2003) proposed a different model to account for low N_2/CO ratio considering the trapping of volatiles in clathrates in which CO is trapped much more easily than N_2. Mousis et al. (2012) considered that cometesimals were formed by the agglomeration of clathrate hydrates, together with other ices. Their model predicts a low abundance of molecular nitrogen in comets as a consequence of the formation of planetesimals at very low temperature (in the 22–47 K range) allowing formation of pure N_2 condensate. Subsequent evolution due to heating from the decay of radiogenic nuclides induces important N_2 losses after the planetesimal formation. Measuring the N_2/CO ratio in comets is thus of great importance to decipher models of planetesimal formation and constrain the physical properties of the solar nebula at the time of their formation. From the detection of N_2 by the ROSINA instrument in the coma of 67P, providing the only direct measurement of the N_2/CO in the coma of a comet so far, Rubin et al. (2015) confirmed that molecular nitrogen appears to be highly depleted in comets compared to the proto-solar value (a factor ~25), suggesting that cometary grains formed at low temperatures (below 30 K).

The detection of strong N_2^+ emission lines in the coma of a relatively bright comet like R2 is a unique opportunity to add a measurement of the N_2/CO ratio for another comet, but also to try to determine the $^{14}N/^{15}N$ isotopic ratio from a direct measurement in N_2, the main reservoir of nitrogen in the early solar system, via N_2^+. We thus decided to observe R2 with UVES, the high resolution optical spectrograph of the European Southern Observatory Very Large Telescope (ESO VLT) to secure a high quality spectrum of the comet over the full optical range. Hereafter, we present the results of those observations.

2. Observations and data reduction

We have been granted a total of five hours of Director's Discretionary Time, with the Ultraviolet-Visual Echelle Spectrograph (UVES) mounted on the ESO 8.2 m UT2 telescope of the VLT to observe R2. We used two different UVES standard settings to cover completely the optical range of the spectrum: the dichroic #1 (390+580) setting covering the range 326 to 454 nm in the blue and 476 to 684 nm in the red, and the dichroic #2 (437+860) setting covering the range 373 to 499 nm in the blue and 660 to 1060 nm in the red. Because of clouds during the second observation performed with the dichroic #1 setting, this observation

was repeated, leading to a total of five exposures. The dates and observing circumstances of the five spectra are summarized in Table 1. For both setups, we used a 0.44″ wide slit, providing a resolving power $R \sim 80\,000$. The smallest slit length of 8″ samples about 14 500 km at the distance of the comet ($\Delta = 2.5$ au).

We reduced the data using the ESO UVES pipeline, combined with custom routines to perform the extraction, cosmic rays removal, and then corrected for the Doppler shift due to the relative velocity of the comet with respect to the Earth. The spectra are calibrated in absolute flux using either the archived master response curve or the response curve determined from a standard star observed close to the science spectrum (both were used for R2 with no significant differences). More details can be found in the UVES ESO pipeline manual[1]. Finally, the continuum, including the sunlight reflected by the cometary dust grains, was removed using a BASS2000 solar spectrum whose slope was corrected to match that of the comet. As a consequence, the final comet spectrum we used only contains the gas component. More details regarding the data reduction can be found in Manfroid et al. (2009).

In addition to the UVES spectra, we also used the TRAPPIST (TRAnsiting Planets and Planetesimals Small Telescope) 60 cm telescopes (Jehin et al. 2011) to monitor the general activity of the comet. The TRAPPIST telescopes are equipped with sets of narrowband filters allowing us to isolate the emission lines of OH, NH, CN, C_3, and C_2 radicals, the CO^+ ion, and several regions of the dust reflected continuum free from gas contamination (Farnham et al. 2000). More details about the TRAPPIST data reduction procedure can be found in Opitom et al. (2015).

3. Results

The spectrum of R2 is very different from what we normally see in other comets at similar distances from the Sun. The optical spectrum of a comet is usually dominated by the emission of radicals such as OH, NH, CN, C_2, C_3, or NH_2. However, the spectrum of R2 is surprisingly dominated by several strong emission bands of the ions CO^+ and N_2^+, and to a lesser extent CO_2^+.
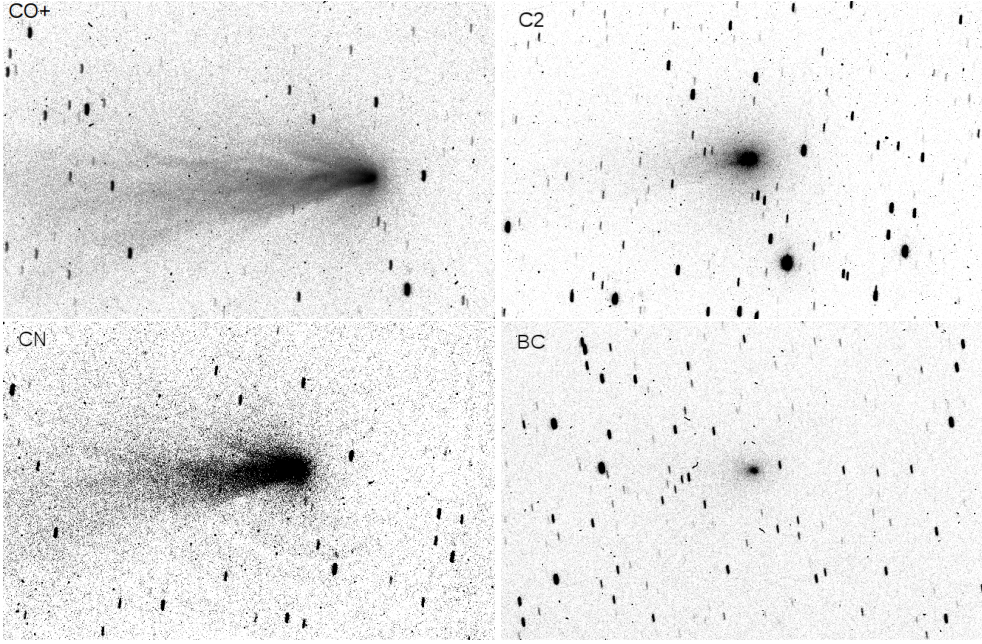
3.1. Narrowband imaging

In Fig. 1, we show images of R2 obtained in early February 2018 (at a heliocentric distance of 2.8 au) with TRAPPIST-South (TS) using the CO^+, C_2, and CN narrowband filters, and an image obtained with TRAPPIST-North (TN) using the narrowband BC filter. The CO^+ coma shows a lot of structures changing night after night, and an enhancement in the anti-sunward direction, as expected for an ion. Instead of showing the usual large diffuse and symmetrical CN coma, the image through the CN filter has a morphology similar to the CO^+ image, indicating that the CN filter is highly contaminated by an ion. This is due to the N_2^+ emission band at 391.4 nm, which lies partially within the bandpass of the CN filter. The lack of the typical CN coma also indicates a low abundance of CN. Similarly, the C_2 image shows some structure due to strong contamination by CO^+ emissions. Because of contamination of the CN and C_2 narrowband filters by other emissions, and the low abundance of those species, which will be discussed further later, we could not reliably compute CN and C_2 production rates from narrowband imaging.

---

[1] ftp://ftp.eso.org/pub/dfs/pipelines/uves/
uves-pipeline-manual-22.17.pdf

Table 1. Observing circumstances of comet C/2016 R2 with VLT/UVES.

Date	r_h (au)	$\dot{r}_h$ (km s^{-1})	Δ (au)	$\dot{\Delta}$ (km s^{-1})	Exptime (s)	UVES setup	UVES slit
2018-02-11T00:27:07.326	2.76	−6.09	2.40	19.7	4800	DIC1-390+580	0.44″ × 8″–0.44″ × 12″
2018-02-13T00:46:23.196	2.76	−5.97	2.43	19.9	4800	DIC1-390+580	0.44″ × 8″–0.44″ × 12″
2018-02-14T00:47:40.759	2.75	−5.91	2.44	20.1	4800	DIC1-390+580	0.44″ × 8″–0.44″ × 12″
2018-02-15T00:23:16.493	2.75	−5.85	2.45	20.1	3000	DIC2-437+860	0.44″ × 10″–0.44″ × 12″
2018-02-16T00:16:08.672	2.75	−5.79	2.46	20.2	3000	DIC2-437+860	0.44″ × 10″–0.44″ × 12″

Fig. 1. TRAPPIST-South images of comet C/2016 R2 obtained with the CO$^+$, C$_2$, and CN narrowband filters and TRAPPIST-North image obtained with the BC narrowband filter on February 10 and 11, 2018 respectively. The images are oriented with north down and east left.

Table 2. $Af\rho$ values of comet C/2016 R2.

Date	r_h (au)	Δ (au)	$Af\rho$(BC) (cm)	$Af\rho$(RC) (cm)	Telescope
2017-12-26	2.96	2.06	752 ± 4	1248 ± 8	TN
2017-12-27	2.95	2.06	–	1158 ± 10	TN
2017-12-27	2.95	2.06	622 ± 11	944 ± 6	TS
2018-01-04	2.92	2.08	631 ± 5	1051 ± 9	TN
2018-01-11	2.88	2.12	536 ± 4	1010 ± 10	TN
2018-01-20	2.84	2.19	520 ± 4	888 ± 3	TN
2018-02-11	2.76	2.41	503 ± 6	829 ± 5	TN
2018-02-13	2.75	2.43	458 ± 6	882 ± 6	TN
2018-03-19	2.65	2.83	408 ± 7	802 ± 8	TN

OH emission at 309 nm was not detected for any of the observing dates with TRAPPIST using the OH narrowband filter. Using simulated OH images produced from a Haser model (Haser 1957) and added to the real images, we could estimate the upper limits of the OH production rates for each observation. Images with the OH filter were taken with TN and TS from December 26, 2017 to February 11, 2018. They all agree with an upper limit of about 5×10^{28} mol. s^{-1} for the OH production rate. This is in agreement with (even though less constraining) the upper limit of 1.1×10^{28} mol. s^{-1} derived by Biver et al. (2018) from observations performed with the Nançay radio telescope between January 2 and March 26, 2018.

Using observations of the comet with narrowband dust filters (BC and RC) performed with both TRAPPIST telescopes between December 26, 2017 and April 8, 2018 we derived $Af\rho$ values to constrain the dust content of the comet (A'Hearn et al. 1984). Those values were computed at a fixed nucleocentric distance of 10 000 km and are reported in Table 2. As can be seen in this table, the $Af\rho$ is decreasing with time even though the comet is getting closer to the Sun. In addition, the $Af\rho$ values are higher in the RC filter than in the BC filter. This is not surprising as the continuum component of the coma of most comets is redder than the solar continuum (see for example Jewitt & Meech 1986). From these observations, we compute a dust reddening as
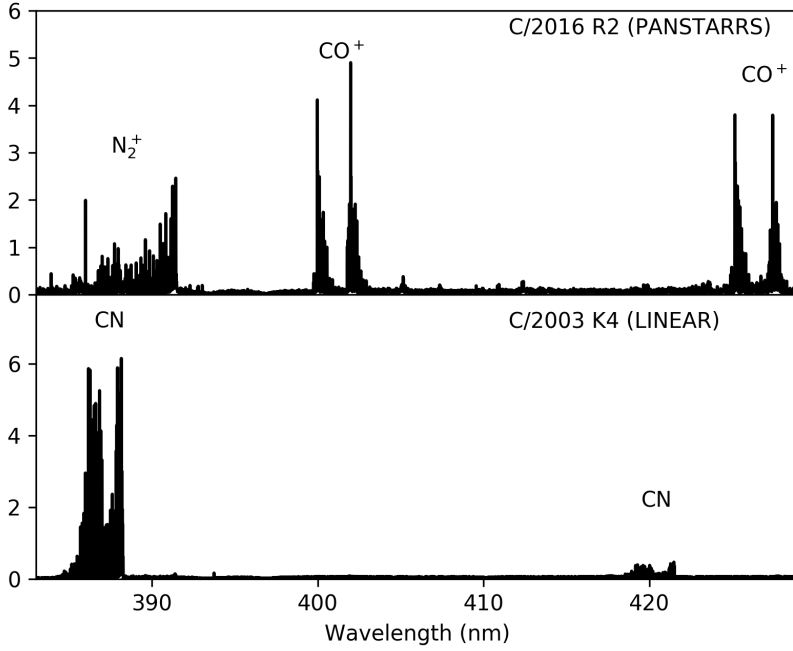
Fig. 2. Comparison of the UVES spectra of C/2016 R2 at 2.8 au and C/2003 K4 at 2.6 au over the 383.0 to 429.0 nm wavelength range. The y-axis has arbitrary units and was chosen independently for both spectra so bright emission features appear with similar intensities.
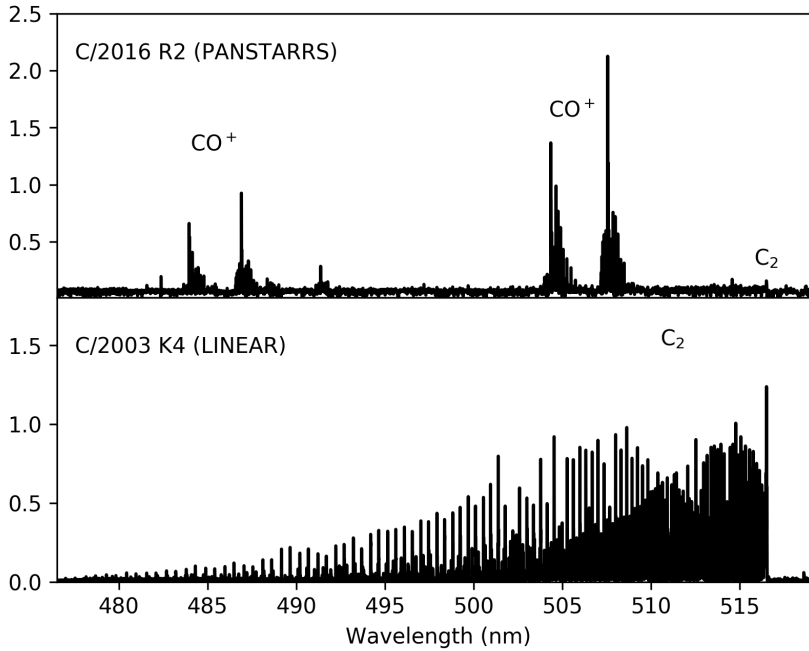

Fig. 3. Comparison of the UVES spectra of C/2016 R2 at 2.8 au and C/2003 K4 at 2.6 au over the 476.5 to 519.5 nm wavelength range. The y-axis has arbitrary units and was chosen independently for both spectra so bright emission features appear with similar intensities.

defined by Jewitt & Meech (1986) between 15% and 24% per 100 nm.

3.2. Detected and non-detected species

Compared to previous observations of this comet with other high resolution spectrographs at optical wavelengths, UVES spectra have the advantage of covering the whole optical range while having the benefit of being mounted on an 8 m class telescope; this allows us to detect fainter emission bands or species. With this spectrum, we confirm the peculiarity of R2, as illustrated in Figs. 2 and 3, where it is compared to the spectrum of comet C/2003 K4 (LINEAR) obtained with the same instrument and spectral resolution and at comparable heliocentric and geocentric distances (Manfroid et al. 2005). The spectrum of C/2003 K4 is dominated by strong CN emission lines around 390 nm and C_2

between 450 and 520 nm, while the spectrum of R2 is dominated by N_2^+ emission below 392 nm and by CO^+ in the 400–620 nm region as already shown by Cochran & McKay (2018). This is also consistent with the CN narrowband images of R2 obtained with TRAPPIST being contaminated by N_2^+ emission lines.

The list of species identified in the UVES spectra is given in Table 3, along with their corresponding transitions. The strongest signatures are those of N_2^+, CO^+, and CO_2^+. In addition to the (4,0), (3,0), (2,0), (4,2), (3,2), (1,0), (2,1), and (1,1) $A^2\Pi - X^2\Sigma$ CO^+ bands reported by Cochran & McKay (2018), we detect the (6,0), (7,1), (5,0), (0,0), (0,1), (1,2), and (0,2) bands of the same system. The (0,0), (1,1), and (0,1) bands of the N_2^+ first negative group ($B^2\Sigma_u^+ - X^2\Sigma_g^+$) are also detected, and we have evidence for the detection of the (0,2) band. Finally, besides N_2^+ and CO^+, we also detect several CO_2^+ bands, as illustrated in Fig. 4. In addition to those three ions, which are dominating the spectrum of R2, we

Table 3. Detected species in the coma of comet C/2016 R2.

Species	Detected bands	Respective band/line wavelengths
CO$^+$	(6,0), (7,1), (5,0), (4,0), (3,0), (2,0), (4,2), (1,0), (2,1), (3,2), (0,0), (1,1), (0,1), (1,2), (0,2) $A^2\Pi - X^2\Sigma$ bands	341, 351, 359, 378, 400, 425, 452, 454, 468, 484, 490, 504, 547, 567, and 619 nm
N$_2^+$	(0,0), (1,1), (0,1) $B^2\Sigma_u^+ - X^2\Sigma_g^+$ bands and a few matching lines for the (0,2) band	391, 389, 428, and 471 nm
CO$_2^+$	(0,0,0) $\tilde{A}^2\Pi_{u,3/2} - (0,0,0)\tilde{X}^2\Pi_{g,1/2}$, (0,0,0) $\tilde{A}^2\Pi_{u,3/2} - (0,0,0)\tilde{X}^2\Pi_{g,3/2}$ the (0,0,0) $\tilde{A}^2\Pi_{u,3/2} - (1,0,0)\tilde{X}^2\Pi_{g,3/2}$, and the (0,0,0) $\tilde{A}^2\Pi_{u,1/2} - (1,0,0)\tilde{X}^2\Pi_{g,1/2}$ bands	351, 350, 366, and 366 nm
CH$^+$	Tentative detection of the (0,0) $A^1\Pi - X^1\Sigma^+$ band	423 nm
CH	(0,0) $A^2\Delta - X^2\Pi$ band and tentative detection of the (0,0) $B^2\Sigma^- - X^2\Pi$ band	431 and 389 nm
CN	(0,0),(1,0) $B^2\Sigma^+ - X^2\Sigma^+$ bands and tentative detection of the (1,1) band	388, 422, and 388 nm
C$_2$	(0,0) $d^3\Pi_g - A^3\Pi_u$ band bandhead (Swan System)	517 nm
C$_3$	(0,0,0)–(0,0,0) and (0,2,0)–(0,0,0) bands and tentative detection of the (0,0,0)–(0,2,0) $\tilde{A}^1\Pi_u - \tilde{X}^1\Sigma_g^+$ band	405, 392, and 407 nm
[OI]	Three forbidden oxygen lines	557.7339, 630.0304, and 636.3776 nm
[NI]	Two forbidden nitrogen lines	519.7900 and 520.0256 nm
[CI]	Three forbidden carbon lines	872.712, 982.411, and 985.024 nm

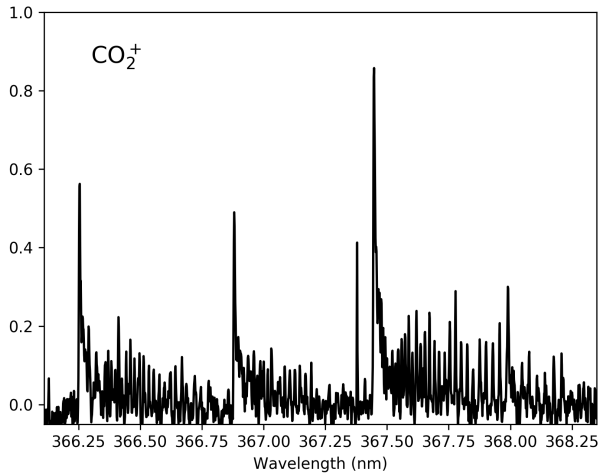**Notes.** OH, OH$^+$, H$_2$O$^+$, and NH$_2$ are not detected.

Fig. 4. Spectrum of C/2016 R2, showing several CO$_2^+$ bands: (0,0,0) $\tilde{A}^2\Pi_{u,3/2} - (1,0,0)\tilde{X}^2\Pi_{g,3/2}$ at 366.3 and 366.9 nm and (0,0,0) $\tilde{A}^2\Pi_{u,1/2} - (1,0,0)\tilde{X}^2\Pi_{g,1/2}$ at 367.4 nm. The *y*-axis has arbitrary units.
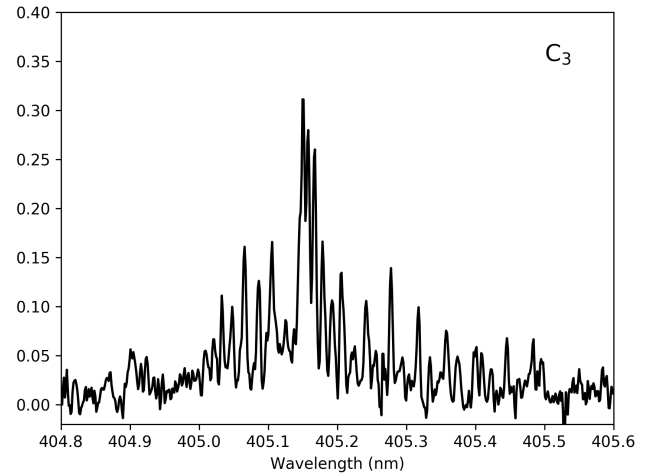

Fig. 5. Spectrum of C/2016 R2, showing the C$_3$ (0,0,0)–(0,0,0) $\tilde{A}^1\Pi_u - \tilde{X}^1\Sigma_g^+$ band around 405 nm. The *y*-axis has arbitrary units.

detect some of the usual CN, C$_3$, and C$_2$ emission lines, but those are much fainter than in other comets at the same distance (see Fig. 9 for the CN (0,0) band, Fig. 5 for C$_3$, and the very faint C$_2$ bandhead visible in Fig. 3). In Fig. 6, the CH (0,0) band is clearly detected, while it was not in the coma of comet C/2003 K4 (LINEAR) observed at a similar heliocentric distance, indicating that R2 seems to be enriched in CH. We also have a tentative identification of a few CH$^+$ lines.

Species that are usually seen in the coma of similarly bright comets but that could not be detected spectra of R2 are as interesting. We searched for OH emission lines to get an indication of the water content of the comet. We looked for matching lines from the $A^2\Sigma^+ - X^2\Pi_i$ (0,1) band around 345 nm without success.

Unfortunately, the setup used did not cover the strongest (0,0) OH emission band around 309 nm. Similarly, we also searched for OH$^+$ lines around 356.5 nm without success. H$_2$O$^+$ has emission lines in the 580–755 nm region, which are regularly detected in the coma of comets (see for example Cochran 2002). Even though, as illustrated in Fig. 7, two faint lines around 618.41 and 619.88 nm (and maybe a third around 614.68 nm) could potentially match the wavelength of H$_2$O$^+$ emission lines, there is no clear evidence for the detection of H$_2$O$^+$ in the coma of R2.

Ultimately, we looked for NH$_2$ emission lines around 570 nm, which we would have expected in such a bright comet at that distance from the Sun. Those lines were for example easily detected in C/2003 K4 (LINEAR) observed under similar circumstances. In Fig. 8, we show several NH$_2$ lines detected in
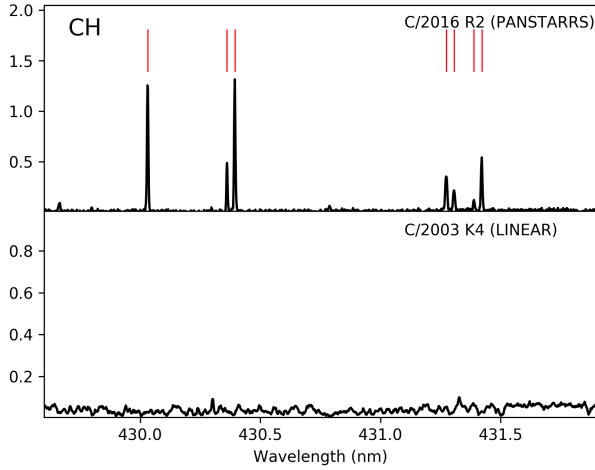
Fig. 6. Comparison of the UVES spectra of C/2016 R2 at 2.8 au and C/2003 K4 at 2.6 au over the 429.5 to 432 nm wavelength range, showing the CH lines from the (0,0) band in R2 (indicated by the vertical red lines) and their absence in K4. The y-axis has arbitrary units and has been chosen to display both spectra on a similar scale.
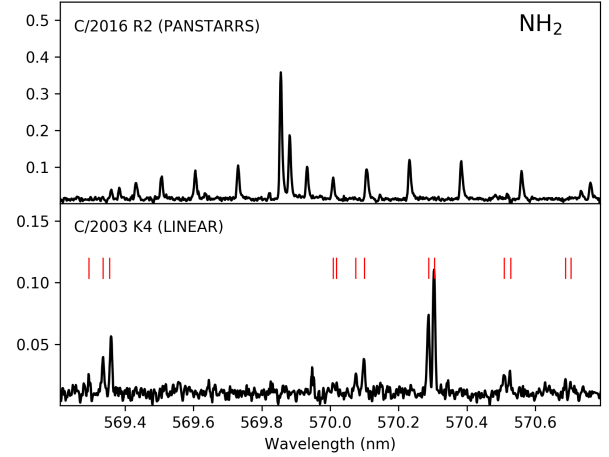

Fig. 7. Spectrum of C/2016 R2 showing the region of H_2O^+ (8,0) band. The red tick marks indicate the wavelength of several of the brightest H_2O^+ lines, which are not clearly detected in C/2016 R2. Most lines detected in this wavelength range belong to the CO^+ (0,2) band. The y-axis has arbitrary units.

Fig. 8. Comparison of the UVES spectra of comets C/2016 R2 at 2.8 au and C/2003 K4 at 2.6 au over the 569.3 to 570.8 nm wavelength range, showing the detection of NH_2 lines in K4 (indicated by the vertical red lines, those lines belong to the $A(0,10,0)–X(0,0,0)$ band) and their non-detection in R2. The y-axis has arbitrary units and has been chosen to display both spectra on a similar scale. Most lines detected in R2 in this wavelength range belong to the CO^+ (1,2) band.
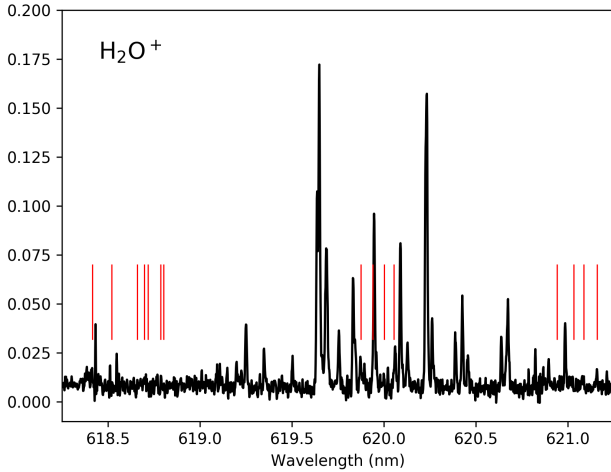
From observations performed with the 2.7 m telescope of the McDonald Observatory in December 2017 at optical wavelengths, Cochran & McKay (2018) could not detect CN, C_2, C_3, or CH, while we see those species about two months later. Although this might be because the comet was further away from the Sun and less active when their observations were done, this is most probably because UVES is mounted on an 8 m telescope, which provides a much higher sensitivity.

Kumar & Shashikiran (2018) reported the detection of H_2O^+ in the coma of R2 using the LISA spectrograph mounted on the 1.2 m telescope of the Mount Abu InfraRed Observatory (MIRO) from observations performed on January 25, 2018, while we do not convincingly detect H_2O^+ emission lines two weeks later. However, the spectrum presented by Kumar & Shashikiran (2018) was obtained at much lower spectral resolution. As illustrated in Fig. 7, in the wavelength range of the H_2O^+ emission lines, we detect numerous emission lines, either belonging to CO^+, identified as sky lines, or unidentified. At low resolution, those could be mistaken for H_2O^+, so we believe that the detection of H_2O^+ by Kumar & Shashikiran (2018) should be taken with caution. We also note that H_2O^+ is not detected by Cochran & McKay (2018) in their November and December 2017 observations.

3.3. Dust-to-gas ratio

Determining absolute gas production rates from high resolution spectra using a small slit is not straightforward, as a correction for slit losses has to be applied. The CN production rate is particularly difficult to measure in the case of R2 because of the N_2^+ (0,0) band partly overlapping with the CN (0,0) band. However, using a model of the CN (0,0) band, combined with a Haser profile to determine the part of the flux encompassed in the slit (and scale lengths from A'Hearn et al. 1995), we estimate a CN production rate of $(3 \pm 1) \times 10^{24}$ mol. s^{-1}. To perform this measurement, we use the first spectrum obtained on February 11 under clear sky conditions. The CN (0,0) band, along with our best model are shown in Fig. 9.

Using this estimate of the CN production rate and the $Af\rho$ measured from TN observations in the BC filter made

K4, which are not detected in the coma of R2. Most lines visible in Fig. 8 in the spectrum of R2 belong to the (1,2) CO^+ band.

Other observations of R2 at optical or radio wavelengths have been performed. de Val-Borro et al. (2018) measured a CO production rate between 1.09 and 1.44×10^{29} mol. s^{-1} from observations at the Arizona Radio Observatory Submillimeter Telescope during the period January 10–16, 2018. This is consistent with what was measured by Biver et al. (2018) from observations with IRAM on January 23–24, 2018. de Val-Borro et al. (2018) did not detect CH_3OH, HCN, CS, H_2CO, or HCO^+. Wierzchos & Womack (2018) also reported that the comet was depleted in HCN compared to CO. This is consistent with the faintness of the CN (0,0) band in the UVES spectra and TRAP-PIST images. Biver et al. (2018) reported the detection of small amounts of HCN as well as the non-detection of OH at radio wavelengths, and confirmed that the comet is strongly depleted in H_2O, CH_3OH, H_2CO, HCN, and H_2S with respect to CO compared to comets observed at similar heliocentric distances.
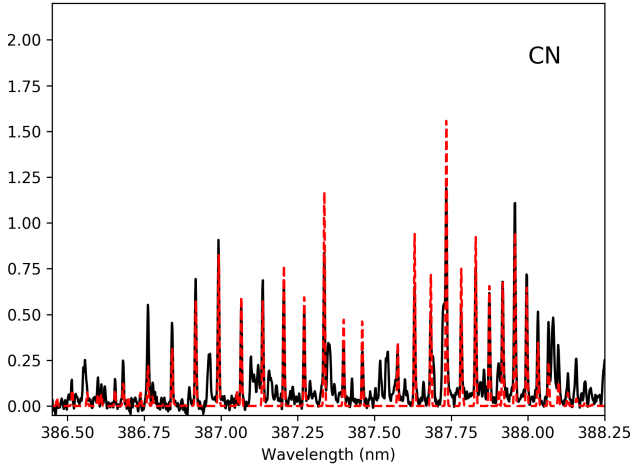
Fig. 9. Spectrum of C/2016 R2 showing the CN (0,0) band in black, overlapped with our best CN model (red dashed line). The *y*-axis has arbitrary units.

Fig. 10. Three forbidden oxygen [OI] lines in comet C/2016 R2 at 557.73 nm (*left panel*) for the green line, and 630.03 nm (*middel panel*), and 636.38 nm (*right panel*) for the red doublet. The cometary oxygen lines are identified by red tick marks, while the dashed blue tick marks indicate the corresponding telluric lines. The *y*-axis is in arbitrary units.

on the same date, we can compute the $Af\rho/Q$(CN) ratio, as a proxy of the dust-to-gas ratio of the comet. We obtain a $log[Af\rho/Q(\text{CN})] = -21.78 \pm 0.14$. Comparing this value to the comets presented in the data set of A'Hearn et al. (1995), and also to more than 30 comets observed with TRAPPIST over the past six years, it is actually higher than for most comets, indicating either a dust-rich or CN-poor comet. We already mentioned previously, and it is illustrated in Fig. 2, that the CN emission in the coma of R2 is faint compared to other comets observed at similar heliocentric distances. Comparing the measured $Af\rho$ value to comets observed at similar heliocentric distance by A'Hearn et al. (1995), R2 is within the range of measured $Af\rho$ values. Biver et al. (2018) compared the $Af\rho$/CO ratio of R2 to comets at similar distances and with available CO abundances and found it particularly low. The question arises whether R2 is rich in CO or poor in dust. Between 2.5 and 3 au from the Sun, H$_2$O, CO, and CO$_2$ can all significantly contribute to the comet activity and their relative contributions vary from comet to comet (see for example Ootsubo et al. 2012). A thorough investigation of the dust-to-gas ratio of comets observed at similar distances, accounting for the contribution of the three species would allow us to decipher whether R2 is actually dust poor, or just very rich in CO. However, simultaneous (or close to simultaneous) and reliable measurements of the H$_2$O, CO, and CO$_2$ abundances in comets observed between 2.5 and 3 au are rare, making such a comparison difficult.

3.4. [NI], [OI] and [CI] forbidden atomic lines

Aside from the molecules mentioned above, we observe emissions from atomic species. The green forbidden oxygen line at 557.73 nm and the red doublet at 630.03 and 636.38 nm are clearly identified (see Fig. 10) and shifted from the corresponding telluric lines owing to the geocentric velocity of the comet. Atomic oxygen in the coma of comets is mainly produced by the photo-dissociation of H$_2$O, CO, and CO$_2$, and, as recently discovered, O$_2$ (Bieler et al. 2015). It has been shown that mixing ratios of CO$_2$/H$_2$O and CO/H$_2$O, which are usually very difficult to determine from the ground, can be derived from observations of the ratio of the green oxygen line to the red doublet (G/R ratio) (Festou & Feldman 1981; McKay et al. 2013; Decock et al. 2013, 2015).
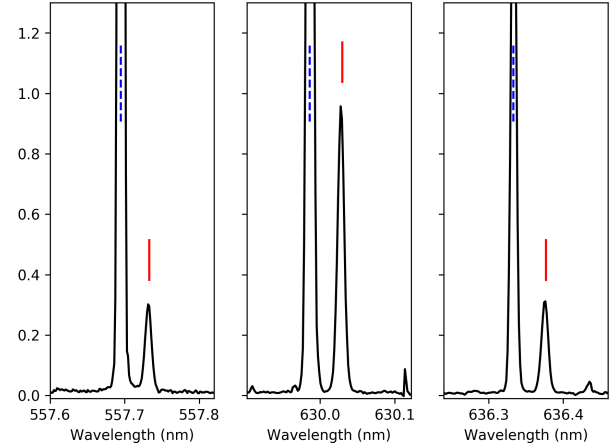
For R2, we measure a G/R ratio of 0.23 ± 0.03 on the average spectrum summing all the flux along the slit. Decock et al. (2013) reported a mean value of 0.11 for their sample of 11 comets, which is about twice lower than what we measure for R2. However, both Decock et al. (2013) and McKay et al. (2015) reported that comets observed at larger heliocentric distance have higher values of the G/R ratio. For example, Decock et al. (2013) reported a ratio of 0.3 for comet C/2001 Q4 (NEAT) observed at 3.73 au and ratios of 0.14 and 0.20 for comet C/2009 P1 (Garradd) observed at 2.9 au and 3.25 au, respectively. McKay et al. (2015) measured a ratio of 0.16 for comet C/2009 P1 (Garradd) observed at 2.88 au and McKay et al. (2012) reported a value of 0.24 for comet C/2006 W3 (Christensen) observed at 3.13 au. The G/R ratio measured for R2 is thus consistent with the ratio measured for other comets observed at large heliocentric distances. The increase of the G/R ratio with the heliocentric distance has been interpreted by the fact that the water sublimation becomes less important at distances larger than 2.5 au so that other volatiles such as CO and CO$_2$ start to contribute more significantly to the comet activity. According to Decock et al. (2013), while for comets observed below 2 au the observed mean G/R ratio of 0.09 is consistent with H$_2$O being the main molecule photodissociated to produce oxygen atoms in metastable state, the high G/R ratio measured at large heliocentric distance indicates that at those distances CO and CO$_2$ are contributing. R2 was observed at ∼2.8 au from the Sun and its spectrum shows strong emission lines of CO$^+$ and CO$_2^+$, while no OH or H$_2$O$^+$ emission lines are convincingly detected. This is consistent with CO and CO$_2$ contributing to drive the activity of R2, implying a higher G/R ratio.

More surprisingly, we detect two lines at 519.79 and 520.03 nm, which we identify as being forbidden nitrogen lines (Wiese et al. 1966), see Fig. 11. To our knowledge, this is the first time those lines are detected in the coma of a comet, even if Singh et al. (1991) mentioned that an unidentified line at 520.1 nm detected in several comets could match the forbidden nitrogen transitions. Those lines are produced by the decay of nitrogen in a metastable state N(^{2}D^0). Nitrogen in this metastable state could be produced in the coma of comets by photodissociation of CN for example (Singh et al. 1991). In the Earth atmosphere, nitrogen in the N(^{2}D^0) state is produced by
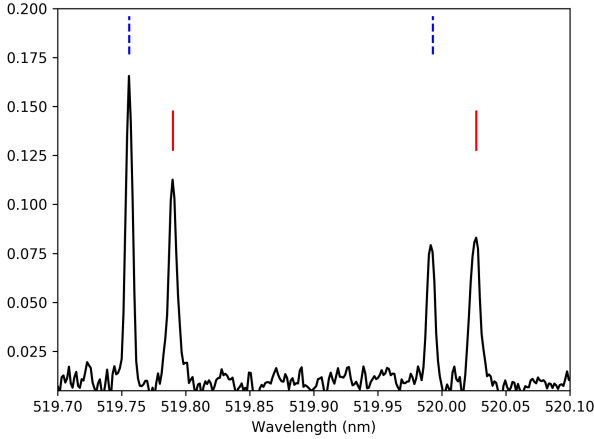
Fig. 11. Spectrum of C/2016 R2 between 519.7 and 520.1 nm. The full red tick marks indicate the two cometary nitrogen forbidden lines at 519.79 and 520.03 nm, while the dashed blue tick marks indicate the corresponding telluric lines. The y-axis is in arbitrary units.

Fig. 12. Spectrum of C/2016 R2 corrected from telluric absorption covering the region of the [CI] forbidden lines at 872.7 nm (*left panel*), 982.4 nm (*middle panel*), and 985.0 nm (*right panel*). The red tick marks indicate the position of the carbon forbidden lines. The y-axis is in arbitrary units.

electron impact dissociation of N_2, electron impact dissociative ionization of N_2, or dissociative electron recombination of N_2^+ among others (Rees & Romick 1985). Cravens & Green (1978) studied airglow phenomenon in the inner coma of comets and, even though this is not included in their model, they suggested that forbidden nitrogen emission at 520 nm could result from the dissociative excitation of N_2. Given the high N_2^+ and the low CN abundances in R2, the dissociative electron recombination of N_2^+, electron impact dissociative ionization of N_2, and/or the electron impact dissociation of N_2 are probably the main contributors to the production of nitrogen atoms in this metastable state. In Fig. 11, we can see that the ratio of the [NI] 519.79 nm to 520.03 nm lines is different for the telluric lines ($\sim$2) and cometary lines ($\sim$1.2). However, this ratio is expected to vary with the electron density (Dopita et al. 1976) and observations of several planetary nebulae by Aller & Walker (1970) for example showed variations between 0.84 and 1.95. Measurements of the ratio in the Earth atmosphere were performed by Sharpee et al. (2005), which found a mean value of 1.759, close to what we measure for telluric lines.

Forbidden [CI] lines at 872.7, 982.4, and 985.0 nm are emitted from C(^{1}D), produced by the photodissociation of neutral C-bearing species, electron-impact on the carbon ground-state C(^{3}P), or dissociative recombination of C-bearing ions such as CO^+. Even though carbon forbidden lines are regularly detected in the coma of comets at UV wavelengths, the 985.0 nm line was previously claimed to have been detected only once in the coma of comet C/1995 O1 (Hale-Bopp) by Oliversen et al. (2002) using a Fabry-Perot technique. In the spectrum of R2, we first observed a relatively strong line at 985.0 nm and a fainter line at 872.7 nm, as illustrated in Fig. 12 (right and left, respectively), but a priori no emission at 982.4 nm. According to Hibbert et al. (1993), the intensity ratio of the 985.0 to 982.4 nm lines should be about 3, so that we should easily detect the 982.4 nm line. After correction for a strong underlying telluric absorption, using the Molecfit tool (Smette et al. 2015), the 982.4 nm forbidden carbon line is clearly detected (Fig. 12, middle part), though its position, width, and intensity cannot be accurately determined. A more thorough modeling of all forbidden lines and their interpretation in terms of mixing ratio of the main contributors to comet activity is out of the scope of this work and will be done in a subsequent paper.
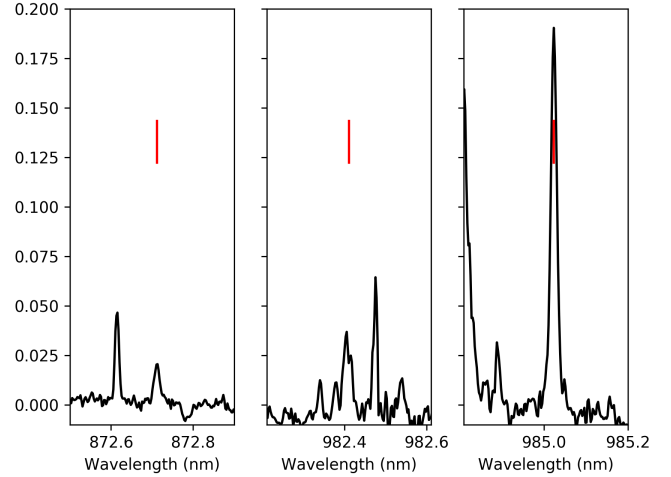
3.5. $N_2^+/CO^+/CO_2^+$ abundance ratios

The N_2^+, CO^+, and CO_2^+ ions have strong detected emissions, such that we can compute the ratios between those species. For CO_2^+, we use the $(0,0,0)\tilde{A}^2\Pi_{u,3/2}-(0,0,0)\tilde{X}^2\Pi_{g,1/2}$ band. Since the majority of the lines identified in that wavelength range are attributed to CO_2^+, we measure the band intensity by fitting a continuum on both sides of the band, subtracting it, and then summing the flux over the entire width of the band. As mentioned before, all spectra were subtracted from the dust continuum. The extra continuum subtraction applied removes any residual continuum component that might be left locally. For N_2^+ and CO^+, we use the (0,0) and (2,0) bands, respectively. Since a non-negligible number of lines not attributed to those species are identified in the wavelength range of the aforementioned bands, we decided to use a different method to measure the intensity of the bands. We first fit and subtract a continuum for each band. In a second time, for each identified line of those two bands, we fit a gaussian and sum all lines of each band. When using the (390 + 580) setting, all three bands of interest are detected in a single setup, allowing us to make the measurements from simultaneous observations.

The N_2^+/CO^+ ratio is computed as

$$\frac{N_2^+}{CO^+} = \frac{g_{CO^+}}{g_{N_2^+}} \frac{I_{N_2^+}}{I_{CO^+}},$$

where $I_{N_2^+}$ and I_{CO^+} are the respective intensities of the N_2^+ and CO^+ bands, $g_{N_2^+}$ is the excitation factor of N_2^+ from Lutz et al. (1993) (7×10^{-2} photons s^{-1} mol.$^{-1}$), and g_{CO^+} is the excitation factor of CO^+ from Magnani & A'Hearn (1986) (3.55×10^{-3} photons s^{-1} mol.$^{-1}$).

The CO_2^+/CO^+ ratio is computed as

$$\frac{CO_2^+}{CO^+} = \frac{g_{CO^+}}{g_{CO_2^+}} \frac{I_{CO_2^+}}{I_{CO^+}},$$

where $I_{CO_2^+}$ and $g_{CO_2^+}$ are the CO_2^+ measured band intensity and excitation factor from Kim (1999) (4.958×10^{-4} photons s^{-1} mol.$^{-1}$), respectively. We measure a N_2^+/CO^+ ratio of 0.06 ± 0.01, in very good agreement

with Cochran & McKay (2018). Only very low upper limits of 1×10^{-5} to 1×10^{-4} for 122P/de Vico, C/1995 O1 (Hale-Bopp), and 153P/Ikeya-Zhang were derived by Cochran et al. (2000); Cochran (2002). Our ratio is higher than the ratio of 0.013 measured for 29P/Schwassmann-Wachmann (Ivanova et al. 2016) but consistent with the ratio of 0.06 measured for C/2002 VQ94 (LINEAR) (Korsun et al. 2014).

For the CO_2^+/CO^+ ratio we obtain a value of 1.1 ± 0.3. Simultaneous measurements of CO^+ and CO_2^+ ions in the coma of comets are scarce. It is then difficult to compare R2 to other comets. Feldman et al. (1997) used the International Ultraviolet Explorer and *Hubble* Space Telescope observations to constrain the CO_2/CO ratio in several comets. For comets for which both species could be detected, they found ratios ranging between 0.67 and 1.69. For two other comets, they could only derive lower limits of 4.6 and 1.8. However, we cannot infer directly the CO_2/CO ratio in the coma of R2 from the CO_2^+/CO^+ ratio. Indeed, CO^+ can be produced both from the photoionization of CO and photodissociative ionization of CO_2. Few studies comparing the efficiencies of both processes have been performed so far, but Huebner & Giguere (1980) suggested that the photodissociative ionization of CO_2 could significantly contribute to the production of CO^+ in the coma of comets, especially in the inner coma. The relative contribution of both mechanisms in the coma of R2 is difficult to assess and would require dedicated modeling. Consequently, we must be cautious while interpreting the CO_2^+/CO^+ and N_2^+/CO^+ abundance ratios measured in the coma of this comet.

In their work, as CO_2^+ was not detected Cochran & McKay (2018) considered that the photoionization of CO is the main source of CO^+ in order to infer a N_2/CO ratio of 0.06 from their measurement of the N_2^+/CO^+ ratio. If we take into account that part of the CO^+ detected in the coma of R2 can be produced by the photodissociative ionization of CO_2 in addition to the photoionization of CO, the N_2/CO of 0.06 reported by Cochran & McKay (2018) would only be a lower limit.

Since we do not detect H_2O^+, we attempt to compute an upper limit of the H_2O^+/CO^+ ratio. We consider the H_2O^+ $\tilde{A}^2A_1 - \tilde{X}^2B_1$ (8,0) band, together with the efficiency factor from Lutz et al. (1993) (4.2×10^{-3} photons s^{-1} mol.$^{-1}$). Since that band is spread over a large wavelength range, over which numerous other emission lines are detected, integrating the flux over the whole wavelength range of the band would not provide a correct upper limit for the H_2O^+ flux. Instead, we define zones spanning 0.015 nm on each side of the center of each line of the band in the cometary atlas of Cochran (2002) and integrate the flux over those areas to have a more realistic estimate of the maximum total flux of the H_2O^+ band. Using this technique, we measure an upper limit of the H_2O^+/CO^+ ratio of 0.4. Lutz et al. (1993) reported H_2O^+/CO^+ ratios varying between 0.6 and 5 for a set of five comets. This is higher than our upper limit for R2, supporting the apparent low water abundance of this comet. However, it is important to keep in mind that the Lutz et al. (1993) measurements have been obtained for comets observed closer to the Sun, where water sublimation is more efficient. Biver et al. (2018) derived an upper limit for the water production rate of R2, leading to an upper limit of the H_2O/CO ratio of about 0.11. This is consistent with our low upper limit for the H_2O^+/CO^+ ratio.

As mentioned earlier, we do not detect NH_2 emission lines in the coma of R2. Nevertheless, deriving a lower limit of the N_2^+/NH_2 ratio would provide an interesting constraint for the

solar nebula nitrogen chemistry. We used the NH_2 $A(0,8,0)$–$X(0,0,0)$ band. In the case of R2, the $A(0,10,0)$–$X(0,0,0)$ band region shown in Fig. 8 contains a large number of CO^+ emissions, making the computation of an upper limit of the NH_2 flux difficult. Similarly to what is done for H_2O^+, we define zones spanning 0.015 nm on each side of the center of each of the brightest lines of the band between 626 and 642 nm and integrated the flux over those areas. We use the fluorescence efficiency from Kawakita & Watanabe (2002) (1.07×10^{-3} photons s^{-1} mol.$^{-1}$). For all the ratios computed before, we assume an identical dependence of the fluorescence efficiencies with the heliocentric distance as r_h^{-2}. However, in the case of NH_2, Kawakita & Watanabe (2002) determined that the fluorescence efficiency actually varies as $r_h^{-1.6}$ and this is what we used. We then estimate the lower limit of the N_2^+/NH_2 ratio to be about 0.4. It must be pointed out that neutral species and ions have different spatial distributions in the coma and caution must then be taken while interpreting column density ratios between ions and neutral species.

3.6. Nitrogen isotopic ratio

Nitrogen is one of the main species in comets because of numerous molecules containing this atom and detected in their coma (NH_3, N_2, HCN, NH_2CHO, HNCO, HNC, CH_3CN, HC_3N, $C_2H_5NO_2$, CH_5N, C_2H_7N). So far it has been possible to measure the $^{14}N/^{15}N$ ratio from CN and NH_2 optical spectra in about 20 comets of various origins. The isotopic ratios measured for these two molecules are in agreement within the error bars: the averaged $^{14}N/^{15}N$ ratio from NH_2 for 18 comets is 135.7 ± 5.9 (Shinnaka et al. 2016) and this agrees with that in CN for 22 comets, i.e., 145.2 ± 5.6 (Manfroid et al. 2009). This ratio was also measured in HCN (the most obvious parent of CN) for comets 17P/Holmes and C/1995 O1 Hale-Bopp with values of 139 and 205, respectively (Bockelée-Morvan et al. 2008). The $^{14}N/^{15}N$ ratio does not seem to vary from one comet to another or with the reservoir of origin. Moreover, long and short period comets present the same ratio (Jehin et al. 2009). It is different from the ratio measured in the Earth's atmosphere (272 for the N_2 molecules according to Nier 1950) or in the presolar nebula (estimated to be 441 from the solar wind, Marty et al. 2011) or 450 from Jupiter's atmosphere (Fouchet et al. 2004). Bockelée-Morvan et al. (2015) provide a detailed discussion about isotopic ratios. The discovery of R2 presenting numerous N_2^+ bright emission lines offered a unique opportunity to detect $^{14}N^{15}N^+$ emission lines and, consequently, to measure the $^{14}N/^{15}N$ isotopic ratio directly in N_2, the main reservoir of nitrogen in the solar nebula.

The first step consists in modeling as accurately as possible the N_2^+ spectrum. The brightest emission lines belong to the (0,0) band of the first negative group, i.e., the $B^2\Sigma_u^+ \rightarrow X^2\Sigma_u^+$ transition with a bandhead at 391.4 nm. A complete modeling of this spectrum would imply a fluorescence model taking into account all the transitions in this system, with the other bands and, possibly, other electronic transitions, both in absorption (of the solar flux) and in emission. We have not (yet) developed such a model but it is possible to do an acceptable modeling using the Boltzmann distribution(s) with parameters fitted to the observed spectrum.

To model the N_2^+ spectrum we first compute the energy levels from the constants published by Wood & Dieke (1938) and Lofthus & Krupenie 1977, their Table 72 and the line energies published by Dick et al. (1978). The Einstein coefficients for
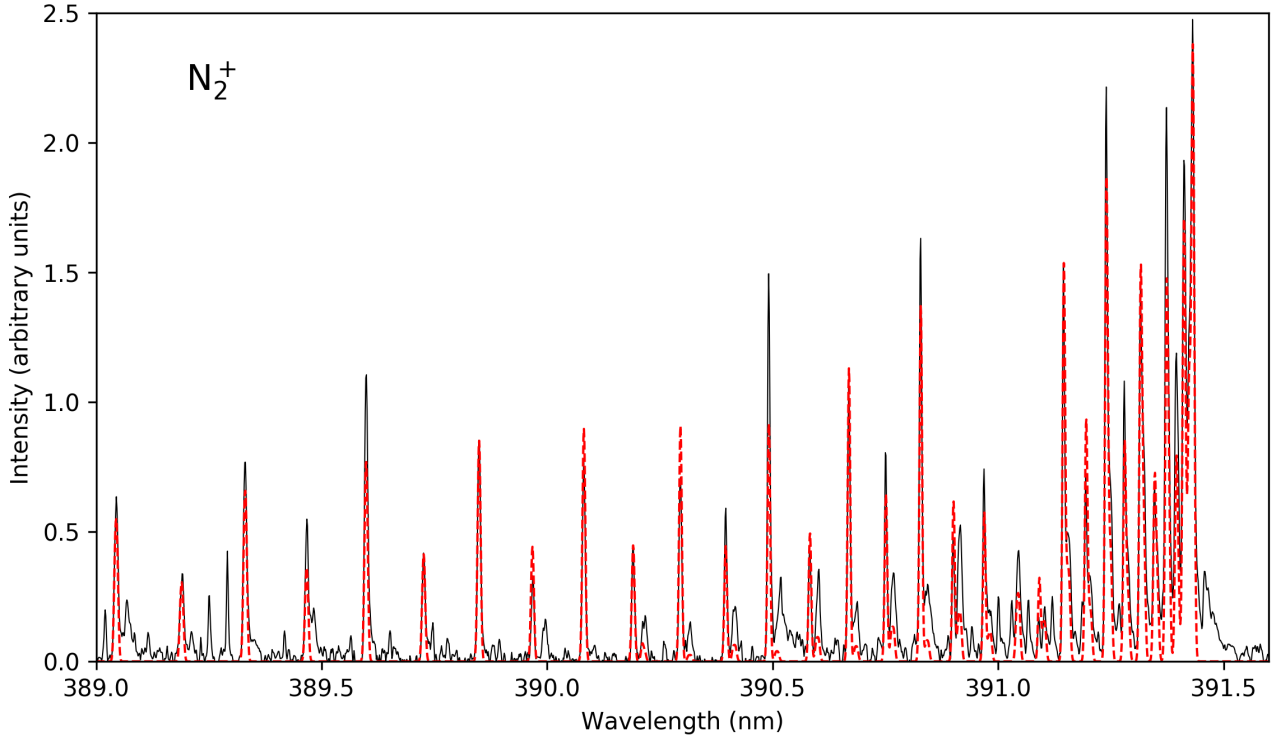
Fig. 13. Observed (black) and synthetic (red dashed) spectra of the N_2^+ (0,0) band of the first negative group in C/2016 R2.

the spontaneous emission, $A_{v'v''}$ come from Jain & Sahni (1967) and the Hönl-London factors from Herzberg (1951) (only P and R lines exist for such a transition). From these data and the observed intensities of the cometary emission lines we compute a Boltzmann diagram to see if this spectrum follows a Boltzmann distribution. We find that the relative populations could be satisfactorily fitted by a double Boltzmann distribution based on two different rotational excitation temperatures, $T_{rot} \sim 45$ K and 860 K; such a two-temperature distribution is not unusual and has been observed for C_2 (e.g., see Rousselot et al. 2012; Nelson et al. 2018 and references therein). From these temperatures we manage to fit the observed spectrum in a satisfying manner by adjusting the relative fraction of both populations. Of course such an approximation does not take into account solar absorption lines but, because of the numerous N_2^+ emission lines, the final fit is satisfactory. Fig. 13 presents the result in the range 389–391.6 nm.

The last step consists in computing a similar spectrum for the $^{14}N^{15}N^+$ isotopolog emission lines. It is done with the help of the line energies published by Wood & Dieke (1938). Only the emission lines belonging to the R branch are computed since this paper does not contain the P branch data (or only very few) because these emission lines are blended with the bright N_2^+ emission lines.

To compute the $^{14}N^{15}N^+$ emission spectrum we use similar rotational temperatures and ratios between them as fitted on N_2^+. Our search for the $^{14}N^{15}N^+$ is based on this spectrum. Figure 14 presents the spectrum computed for $^{14}N/^{15}N = 100$ (i.e., an intensity ratio of 50 with the N_2^+ emission lines). As it can be seen no $^{14}N^{15}N^+$ emission line is clearly identified. An estimate of the noise in the observational spectrum leads to about 0.02 (arbitrary) intensity units, to be compared to the maximum intensity of the $^{14}N^{15}N^+$ synthetic spectrum. Our conclusion is that only a lower limit for the $^{14}N/^{15}N$ ratio can be computed. This lower limit is roughly equal to 100.

3.7. Dynamical history of R2

We outlined several times that R2 has a very unusual composition, showing strong emission lines of N_2^+, CO^+, and CO_2^+, but no detected water or any of its dissociation product. In order to try to reach a better understanding of the origin of this comet, we decided to have a closer look at its dynamical history.

As we mentioned before, R2 is a nearly-isotropic comet originating from the Oort cloud, belonging to the subclass of returning objects; i.e., it is not the first time that this object has visited the inner region of the solar system (Levison 1996; Dones et al. 2015). According to Fernández (2005), the computation of the original semimajor axis, a_{org}, and the orbital energy, χ_{org}, is of great interest for long period comets since these parameters are vital to assess the place an object comes from and to determine its dynamical age, i.e., the average number of revolutions it has performed in the inner planetary region. This is particularly interesting in the case of R2, given its peculiar chemical composition.

By definition, the original orbit of a comet is the orbit a comet had before entering the planetary region with respect to the barycenter of the solar system; Fernández (2005) provides further details about the computation of original orbits. R2 has an original reciprocal semimajor axis of $1/a_{org} = 0.00129$ au^{-1} (cf. the IAU/MPC Data Base[2]). From observations and theoretical studies, Fernández (2005) showed that a comet with such a reciprocal semimajor axis (or an equivalent orbital energy of $\chi_{org} = -0.00129$ au^{-1}) performs about ten revolutions before suffering an hyperbolic ejection ($\chi_{org} > 0$). In order to assess the number of revolutions R2 has completed, we decided to study its recent dynamical history through numerical simulations, as it has been done before by other authors for the study of long period comets (see, for example, Hui 2018; Hui et al. 2018, for
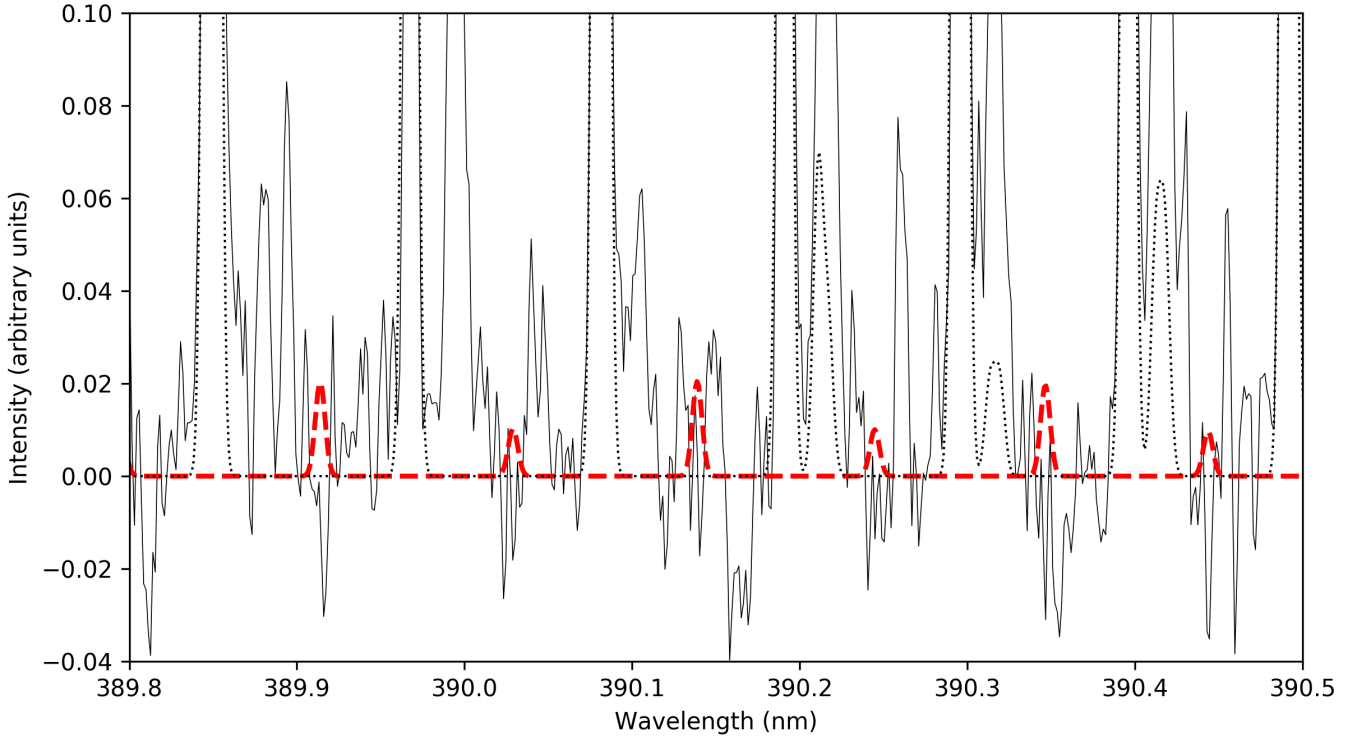
---

[2] https://www.minorplanetcenter.net/db_search

Fig. 14. Zoom of the observed spectrum (black) of C/2016 R2 and the ^{14}N^{15}N$^+$ synthetic spectrum computed for ^{14}N/^{15}N = 100 (dashed red curve). The dotted line represents the N$_2^+$ synthetic spectrum. In this part of the spectrum only the R lines (the brightest ones) of ^{14}N^{15}N$^+$ are represented in the synthetic spectrum.

Jupiter family comets; Pozuelos et al. 2018; Fernández & Sosa 2015, and for activated asteroids; Novaković et al. 2014; and Moreno et al. 2017).

In order to do this study, we use numerical integrations in the heliocentric frame, where the current time is set as the last perihelion passage, i.e., May 9, 2018. We extend our integrations 3×10^5 yr backward. We use the numerical package REBOUND (Rein & Liu 2012), with the integrator algorithm MERCURIUS, which is an hybrid integrator that combines a fast and unbiased symplectic Wisdom-Holman integrator, WHFAST (Rein & Tamayo 2015), and a high accuracy non-symplectic integrator with adaptive time-stepping algorithm that handles close encounters, IAS15 (Rein & Spiegel 2015). Because of the accumulation of errors during the numerical integrations, the dynamical evolution of a long period comet through successive passages by the planetary region is a stochastic process in which in every perihelion passage the comet meets a planetary configuration completely different from the previous one. To solve this, we perform a statistical study in which, in addition to the nominal orbit of the comet, the orbital evolution of a set of clones on orbits corresponding to the uncertainty is also followed. For this purpose, we generate 1000 clones based on the covariance matrix of the orbital elements (Chernitsov et al. 1998).

In order to make the problem tractable with ordinary computational facilities, we split our 1000 clones into 10 sets of 100 clones. The set of orbital elements and the covariance matrix of the orbit of R2 are published together in the NASA/JPL Small-Body browser (JPL 20). The initial timestep is set to five days and the computed orbital evolution is stored every year for each clone. The Sun, the eight planets, and Pluto are included in the simulation. We neglect both Galactic tide and gravitational effects of stars passing close to the Sun; these are the two main effects that contribute to ejecting comets from the Oort cloud

to the inner solar system. This assumption is valid because both effects are almost null for objects having semimajor axis well below $a \sim 20\,000$ au (Souchay & Dvorak 2010; Dones et al. 2015). The action of non-gravitational forces might have a significant effect for long period comets approaching the Sun to less than a few tenths of au. However, the evaluation of these forces for long period comets is difficult since they have not been observed in a second apparition during which variations of the time of the perihelion passage could be detected. Thus, for simplicity, we do not include galactic tide, gravitational effects of stars passing close to the Sun, and non-gravitational forces in our simulations.

The orbital evolution of R2 and its 1000 clones in terms of reciprocal semimajor axis, $1/a$, eccentricity, e, and heliocentric distance in the past 1.5×10^5 yr is shown in Fig. 15. Our study shows that in a period between $-(50$ and $100)$ kyr 95% of the clones experience a dramatic change in their orbits, suffering hyperbolic ejections, i.e., $e > 1$ and $1/a < 0$. Therefore, we consider the upper limit of the time during which R2 has been orbiting in its current orbit to be on the order of 150 kyr. Moreover, our simulations show that 72.9% of the clones pass through perihelion only three times, 23.9% pass four times, 2.8% pass five times, and 0.4% pass six times. In all cases, the perihelion distances are in the range 2.6–3.2 au. These results show that R2 is in a dynamical state of evolution within the limits of "young" and "middle-age" as defined in Fernández (2005).

This study indicates that R2 had a relatively quiet recent dynamical history. As a consequence, it does not seem that its peculiar composition is related to its recent orbital evolution. The comet is not at its first passage through the planetary region, so it is not releasing unusual amounts of highly volatile species because it is approaching the Sun for the first time, but it has not been heavily processed due to repeated passages close to the
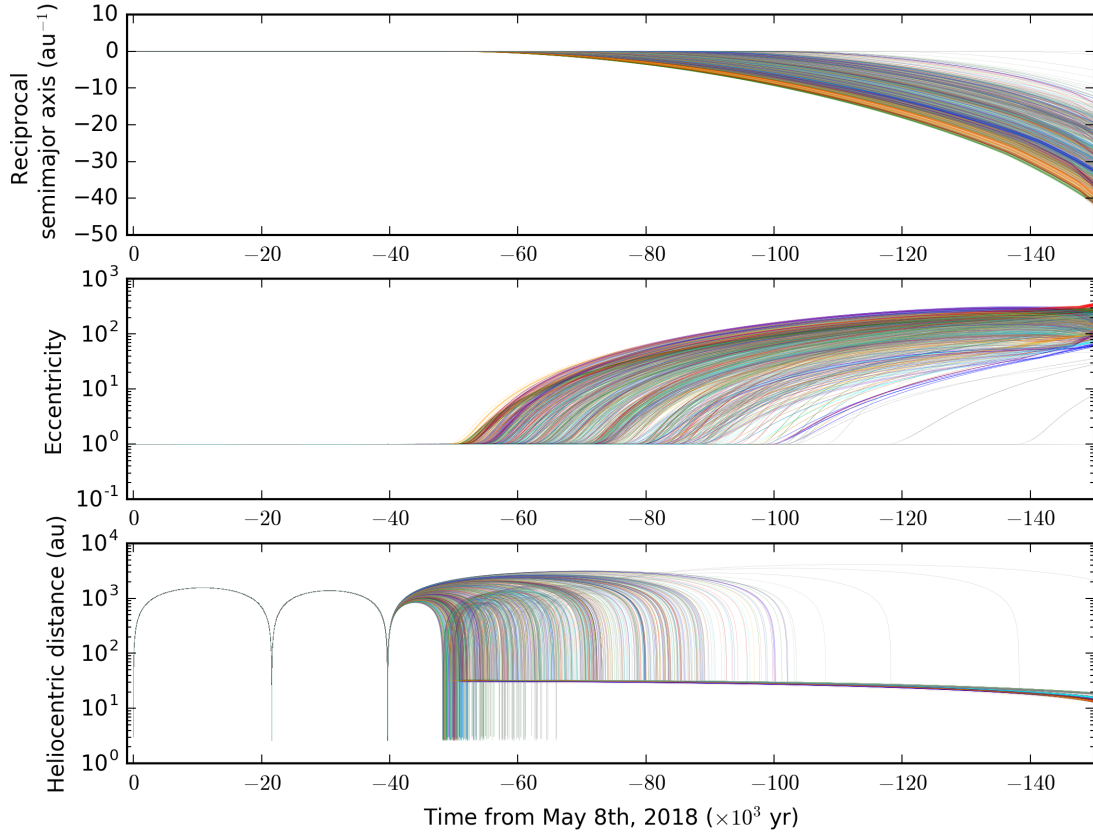
Fig. 15. Orbital evolution of C/2016 R2 and 1000 clones over 1.5×10^5 yr backward in time from last perihelion passage on May 9, 2018. Different colors represent different sets of 100 clones (see text for details). *From the top to the bottom panels*: reciprocal semimajor axis, eccentricity, and heliocentric distance.

Sun either. This indicates that, while the orbit of R2 is similar to many other Oort Cloud comets, its composition is intrinsically different.

4. Discussion and conclusions

In this work, we present high resolution optical observations of comet C/2016 R2 (PanSTARRS) performed with the UVES instrument at the VLT, complemented by narrowband imaging obtained with the TRAPPIST telescopes. R2 has a very peculiar chemical composition, with strong N_2^+, CO^+, and CO_2^+ emission lines in the optical, faint CN, C_3, and C_2, and no detected OH, OH^+, or H_2O^+, suggesting a comet rich in N_2 and CO but relatively poor in water. The comet also has clearly detected CH emissions. Table 4 summarizes the ratios measured in the coma of R2. The non-detection of NH_2 seems to suggest that most of the nitrogen content of R2 is concentrated in N_2 with a lower limit of the N_2^+/NH_2 ratio of 0.4. Such a high N_2^+/NH_2 ratio might put strong constraints on the origin of R2 through adequate modeling (Womack et al. 1992). In some ways, R2 is similar to comets 29P/Schwassmann-Wachmann and C/2002 VQ94 (LINEAR), which are both distant active comets displaying clear N_2^+ and CO^+ emission lines.

Because we detect very strong N_2^+ bands, we attempted to measure the $^{14}N/^{15}N$ isotopic ratio from N_2^+ directly for the first time. We could derive a lower limit of the $^{14}N/^{15}N$ isotopic ratio of about 100, which is consistent with the values measured for comets from CN and NH_2 (Manfroid et al. 2009; Shinnaka et al. 2016).

Table 4. Ratios measured in the coma of R2.

Species	Ratio
N_2^+/CO^+	0.06 ± 0.01
CO_2^+/CO^+	1.1 ± 0.3
H_2O^+/CO^+	<0.4
N_2^+/NH_2	>0.4
$\log[Af\rho/Q(CN)]$	-21.78 ± 0.14

We determine an upper limit of about 0.4 for the H_2O^+/CO^+ ratio, indicating a low water abundance in the coma of R2. This is in agreement with our measurement of the ratio of the green oxygen forbidden line at 557.73 nm to the red doublet at 630.03 and 636.37 nm. This quantity can be linked to the mixing ratios of CO/H_2O and CO_2/H_2O. We measure a G/R ratio of 0.23, which is consistent with what has been measured by Decock et al. (2013) for comets observed at large distances from the Sun (>3.0 au), when water sublimation is less efficient and CO and CO_2 are significantly contributing to the cometary activity.

For the first time, we clearly detected the [NI] forbidden lines at 519.79 and 520.02 nm in the coma of a comet. These lines are the result of the decay of nitrogen in a metastable state most probably produced in this case by the dissociative electron recombination of N_2^+, electron impact dissociative ionization of N_2, and/or the electron impact dissociation of N_2. We conducted a search in our database of high resolution spectra of a dozen comets observed with UVES over the past 15 years. We do not

detect the [NI] lines in any of those comets, among which some have been observed under circumstances similar to those of R2. The unusually high abundance of molecular nitrogen in the coma of R2 might then explain why we detect the [NI] lines in this particular comet and not in others.

The presence of highly volatile species such as N$_2$ or CO in unusually high amounts while other species like water, CN, or NH$_2$ are depleted is difficult to explain. One could wonder whether this comet has undergone only very minor processing since its formation, for example. However, our analysis of its dynamical history shows that R2 is a dynamically middle-aged comet coming from the Oort cloud, having crossed the planetary region at least three times in the past, with perihelion distances of around 2.5–3.0 au. Therefore the peculiar composition of its coma cannot be explained by the fact that it is releasing highly volatile gases far away from the Sun on its first perihelion passage, even though it probably did not undergo strong thermal processing due to a close encounter with the Sun.

Another hypothesis is that the origin of its peculiarity might then be intrinsic and linked to the conditions prevailing in the solar nebula at the time of its formation, to the distance from the Sun, or the time at which it formed. Since we detect significant CO$_2^+$ emission lines, we cannot derive the N$_2$/CO ratio from our measurement of the N$_2^+$/CO$^+$. However, we can set a lower limit of 0.06. This value is about ten times higher than that measured in comet 67P, which was interpreted as an indication of a lower limit of 24 K for the temperature experienced by the grains when they agglomerated to form 67P (Rubin et al. 2015). This interpretation is based on the results of laboratory experiments published by Bar-Nun et al. (2007) and their estimation of the N$_2$/CO depletion factor at three different temperatures (24, 27, and 30 K). For 24 K this depletion factor was found to be ∼19, and this value is within the range of that observed in 67P (25.4 ± 8.9). Because this depletion factor increases between 24 K and 27 K, Rubin et al. (2015) considered this work as indicative of a lower limit of 24 K for the temperature experienced by the grains when they agglomerated to form 67P. For R2 we estimate a N$_2$/CO ratio one order of magnitude above that measured for 67P, with a large amount of N$_2$ and CO, indicating that the temperature experienced by the grains when they agglomerated was lower than 24 K based on the measured efficiency of gas trapping in water ice. It should, nevertheless, be pointed out that different attempts to measure N$_2$/CO from N$_2^+$/CO$^+$ with ground-based facilities (Cochran et al. 2000; Cochran 2002) in different comets (153P/Ikeya-Zhang, C/1995 O1 Hale-Bopp and 122P/1995 S1 de Vico) provided upper limits for the N$_2$/CO ratio to be one order of magnitude lower than the ratio measured in the coma of 67P. An observational bias cannot be excluded because these attempts to measure this ratio are based on a very different observational technique compared to the in situ ROSINA measurements. These results, nevertheless, seem to indicate that both 67P and R2 are enriched in N$_2$ compared to most comets, the last showing the strongest enrichment in N$_2$. At the end we can only speculate that the temperature of the formation region of R2 was lower than that of 67P, but it is hard to be more accurate on this point.

Alternatively, Biver et al. (2018) suggested that R2 could be a collisional fragment of a Kuiper belt object (KBO). Indeed, some Kuiper belt objects such as Pluto or Eris have N$_2$-rich surfaces. Large KBOs are differentiated and the radiogenic heating they undergo would release highly volatile gases, which then re-condenses in the outer layers, enriching those layers in volatiles such as N$_2$ or CO. Another clue that could point toward R2 being a KBO fragment is the strong CH emission we detected, which could point to a relatively high methane content. Kuiper belt objects like Pluto and Eris have been shown to have a surface rich in methane. However, even though it is dynamically possible, the likelihood of a KBO fragment ending up on an Oort Cloud orbit should be investigated. In conclusion, more modeling is needed to understand the origin of the peculiar chemical composition of R2 in terms of its place and conditions of formation as well as its evolutionary path.

References

A'Hearn, M. F., Schleicher, D. G., Millis, R. L., Feldman, P. D., & Thompson, D. T. 1984, AJ, 89, 579

A'Hearn, M. F., Millis, R. C., Schleicher, D. O., Osip, D. J., & Birch, P. V. 1995, Icarus, 118, 223

Aller, L. H., & Walker, M. F. 1970, ApJ, 161, 917

Bar-Nun, A., Notesco, G., & Owen, T. 2007, Icarus, 190, 655

Bieler, A., Altwegg, K., Balsiger, H., et al. 2015, Nature, 526, 678

Biver, N., Bockelée-Morvan, D., Paubert, G., et al. 2018, A&A, 619, A127

Bockelée-Morvan, D., Biver, N., Jehin, E., et al. 2008, ApJ, 679, L49

Bockelée-Morvan, D., Calmonte, U., Charnley, S., et al. 2015, Space Sci. Rev., 197, 47

Chernitsov, A. M., Baturin, A. P., & Tamarov, V. A. 1998, Solar Syst. Res., 32, 405

Cochran, A. L. 2002, ApJ, 576, L165

Cochran, A. L., & McKay, A. J. 2018, ApJ, 854, L10

Cochran, A. L., Cochran, W. D., & Barker, E. S. 2000, Icarus, 146, 583

Cravens, T. E., & Green, A. E. S. 1978, Icarus, 33, 612

de La Baume Pluvinel, A., & Baldet, F. 1911, ApJ, 34, 89

de Val-Borro, M., Milam, S. N., Cordiner, M. A., et al. 2018, ATel, 11254

Decock, A., Jehin, E., Hutsemékers, D., & Manfroid, J. 2013, A&A, 555, A34

Decock, A., Jehin, E., Rousselot, P., et al. 2015, A&A, 573, A1

Dick, K. A., Benesch, W., Crosswhite, H. M., et al. 1978, J. Mol. Spectr., 69, 95

Dones, L., Brasser, R., Kaib, N., & Rickman, H. 2015, Space Sci. Rev., 197, 191

Dopita, M. A., Mason, D. J., & Robb, W. D. 1976, ApJ, 207, 102

Farnham, T. L., Schleicher, D. G., & A'Hearn, M. F. 2000, Icarus, 147, 180

Feldman, P. D., Festou, M. C., Tozzi, P., & Weaver, H. A. 1997, ApJ, 475, 829

Fernández, J. A. 2005, Astrophys. Space Sci. Lib. (Dordrecht: Springer), 328

Fernández, J. A., & Sosa, A. 2015, Planet. Space Sci., 118, 14

Festou, M., & Feldman, P. D. 1981, A&A, 103, 154

Fouchet, T., Irwin, P. G. J., Parrish, P., et al. 2004, Icarus, 172, 50

Greenstein, J. L. 1962, ApJ, 136, 688

Haser, L. 1957, Bull. Soc. R. Sci. Liège, 43, 740

Herzberg, G. 1951, Am. J. Phys. 19, 390

Hibbert, A., Biemont, E., Godefroid, M., & Vaeck, N. 1993, A&AS, 99, 179

Huebner, W. F., & Giguere, P. T. 1980, ApJ, 238, 753

Hui, M.-T. 2018, AJ, 156, 73

Hui, M.-T., Jewitt, D., & Clark, D. 2018, AJ, 155, 25

Iro, N., Gautier, D., Hersant, F., Bockelée-Morvan, D., & Lunine, J. I. 2003, Icarus, 161, 511

Ivanova, O. V., Luk'yanyk, I. V., Kiselev, N. N., et al. 2016, Planet. Space Sci., 121, 10

Ivanova, O. V., Picazzio, E., Luk'yanyk, I. V., Cavichia, O., & Andrievsky, S. M. 2018, PASS, 157, 34

Jain, D. C., & Sahni, R. C. 1967, Int. J. Quant. Chem., 1, 721

Jehin, E., Gillon, M., Queloz, D., et al. 2011, The Messenger, 145, 2

Jehin, E., Manfroid, J., Hutsemékers, D., Arpigny, C., & Zucconi, J.-M. 2009, Earth Moon Planets, 105, 167

Jewitt, D., & Meech, K. J. 1986, ApJ, 310, 937

Kawakita, H., & Watanabe, J.-I. 2002, ApJ, 572, L177

Kim, S. J. 1999, Earth Planets Space, 51, 139

Korsun, P. P., Ivanova, O. V., & Afanasiev, V. L. 2008, Icarus, 198, 465
Korsun, P. P., Rousselot, P., Kulyk, I. V., Afanasiev, V. L., & Ivanova, O. V. 2014, Icarus, 232, 88
Kumar, V., & Shashikiran, G. 2018, EPSC Abstr. Eur. Planet. Sci. Congr. 2018, 12
Levison, H. F. 1996, in Completing the Inventory of the Solar System, eds. T. Rettig, & J. M. Hahn, ASP Conf. Ser. 107, 173
Lofthus, A., & Krupenie, P. H. 1977, J. Phys. Chem. Ref. Data, 6, 113
Lutz, B. L., Womack, M., & Wagner, R. M. 1993, ApJ, 407, 402
Magnani, L., & A'Hearn, M. F. 1986, ApJ, 302, 477
Manfroid, J., Jehin, E., Hutsemékers, D., et al. 2005, A&A, 432, L5
Manfroid, J., Jehin, E., Hutsemékers, D., et al. 2009, A&A, 503, 613
Marty, B., Chaussidon, M., Wiens, R. C., Jurewicz, A. J. G., & Burnett, D. S. 2011, Science, 332, 1533
McKay, A. J., Chanover, N. J., Morgenthaler, J. P., et al. 2012, Icarus, 220, 277
McKay, A. J., Chanover, N. J., Morgenthaler, J. P., et al. 2013, Icarus, 222, 684
McKay, A. J., Cochran, A. L., DiSanti, M. A., et al. 2015, Icarus, 250, 504
Moreno, F., Pozuelos, F. J., Novaković, B., et al. 2017, ApJ, 837, L3
Mousis, O., Guilbert-Lepoutre, A., Lunine, J. I., et al. 2012, ApJ, 757, 146
Nelson, T., Cochran, A. L., & Western, C. 2018, J. Phys. Chem. A, 122, 8020
Nier, A. O. 1950, Phys. Rev., 77, 789
Novaković, B., Hsieh, H. H., Cellino, A., Micheli, M., & Pedani, M. 2014, Icarus, 231, 300
Oliversen, R. J., Doane, N., Scherb, F., Harris, W. M., & Morgenthaler, J. P. 2002, ApJ, 581, 770
Ootsubo, T., Kawakita, H., Hamada, S., et al. 2012, ApJ, 752, 15
Opitom, C., Jehin, E., Manfroid, J., et al. 2015, A&A, 574, A38
Owen, T., & Bar-Nun, A. 1995, Icarus, 116, 215
Pozuelos, F. J., Jehin, E., Moulane, Y., et al. 2018, A&A, 615, A154
Rees, M. H., & Romick, G. J. 1985, J. Geophys. Res., 90, 9871
Rein, H., & Liu, S.-F. 2012, A&A, 537, A128
Rein, H., & Spiegel, D. S. 2015, MNRAS, 446, 1424
Rein, H., & Tamayo, D. 2015, MNRAS, 452, 376
Rousselot, P., Jehin, E., Manfroid, J., & Hutsemékers, D. 2012, A&A, 545, A24
Rubin, M., Altwegg, K., Balsiger, H., et al. 2015, Science, 348, 232
Sharpee, B. D., Slanger, T. G., Cosby, P. C., & Huestis, D. L. 2005, Geophys. Res. Lett., 32, L12106
Shinnaka, Y., Kawakita, H., Jehin, E., et al. 2016, MNRAS, 462, S195
Singh, P. D., D'Ealmeida, A. A., & Huebner, W. F. 1991, Icarus, 90, 74
Smette, A., Sana, H., Noll, S., et al. 2015, A&A, 576, A77
Souchay, J., & Dvorak, R. 2010, Dynamics of Small Solar System Bodies and Exoplanets (Berlin, Heidelberg: Springer)
Weryk, R., & Wainscoat, R. 2016, Central Bureau Electronic Telegrams, 4318
Wierzchos, K., & Womack, M. 2017, Central Bureau Electronic Telegrams, 4464
Wierzchos, K., & Womack, M. 2018, AJ, 156, 34
Wiese, W. L., Smith, M. W., & Glennon, B. M. 1966, Atomic transition probabilities. Hydrogen through Neon. A critical data compilation (Washington, DC: U.S. Government Printing Office)
Womack, M., Wyckoff, S., & Ziurys, L. M. 1992, ApJ, 401, 728
Wood, R. H., & Dieke, G. 1938, JCP, 6, 734
Wyckoff, S., & Theobald, J. 1989, Adv. Space Res., 9, 157